









# Upstream Plasma Waves and Downstream Magnetic Reconnection at a Reforming Quasi-parallel Shock

Quanming Lu<sup>1,2,3</sup> , Ao Guo<sup>1,2,3</sup> , Zhongwei Yang<sup>4</sup> , Rongsheng Wang<sup>1,2,3</sup> , San Lu<sup>1,2,3</sup> , Rui Chen<sup>1,2,3</sup> , and Xinliang Gao<sup>1,2,3</sup>

<sup>1</sup> Deep Space Exploration Laboratory, School of Earth and Space Sciences, University of Science and Technology of China, Hefei 230026, People's Republic of China; [qmlu@ustc.edu.cn](mailto:qmlu@ustc.edu.cn)

<sup>2</sup> CAS Center for Excellence in Comparative Planetology, CAS Key Lab of Geospace Environment, Hefei 230026, People's Republic of China

<sup>3</sup> Collaborative Innovation Center of Astronautical Science and Technology, Harbin, People's Republic of China

<sup>4</sup> State Key Laboratory of Space Weather, National Space Science Center, Chinese Academy of Sciences, Beijing 100190, People's Republic of China

Received 2023 November 2; revised 2024 January 24; accepted 2024 January 29; published 2024 March 13

## Abstract

With the help of a two-dimensional particle-in-cell simulation model, we investigate the long-time evolution (near  $100\Omega_{i0}^{-1}$ , where  $\Omega_{i0}$  is the ion gyrofrequency in the upstream) of a quasi-parallel shock. Some of the upstream ions are reflected by the shock front, and their interactions with the incident ions excite low-frequency magnetosonic waves in the upstream. Detailed analyses have shown that the dominant wave mode is caused by the resonant ion–ion beam instability, and the wavelength can reach tens of ion inertial lengths. Although these plasma waves are directed toward the upstream in the upstream plasma frame, they are brought by the incident plasma flow toward the shock front, and their amplitude is enhanced during the approaching. The interaction of the upstream plasma waves with the shock leads to the cyclic reformation of the shock front, and the reformation period is slightly larger than  $10\Omega_{i0}^{-1}$ . When crossing the shock front, these large-amplitude plasma waves are compressed and evolve into current sheets in the transition region of the shock. At last, magnetic reconnection occurs in these current sheets, accompanying the generation of magnetic islands. Simultaneously, there still exist plasma waves of another kind, with the wavelength of several ion inertial lengths in the ramp of the shock, which are excited by the nonresonant ion–ion beam instability. The current sheets in the transition region are distorted and broken into several segments when the plasma waves of this kind are transmitted into the downstream, where magnetic reconnection and the generated islands have a much smaller size. No obvious ion flow can be observed around some X-lines produced in the magnetic reconnection, and this implies that electron-only reconnection may occur.

*Unified Astronomy Thesaurus concepts:* Space plasmas (1544); Plasma physics (2089); Solar magnetic reconnection (1504); Planetary bow shocks (1246)

## 1. Introduction

Magnetic reconnection, which is accompanied with a topological change in magnetic field lines, converts magnetic energy into plasma kinetic energy and is believed to be the underlying mechanism for explosive phenomena in the solar atmosphere, planetary magnetosphere, and laboratory plasma (Biskamp 2000; Birn & Priest 2007; Yamada et al. 2010; Zhang et al. 2012; Wang & Lu 2019). A prerequisite for the occurrence of magnetic reconnection is the formation of a current sheet, where the component of the magnetic field along the outflow direction is opposite on two sides (Parker 1957; Sweet 1958; Vasyliunas 1975; Birn et al. 2001; Fu et al. 2006). In the Earth's magnetosphere, the magnetotail and dayside magnetopause are the two most frequent sites where magnetic reconnection can occur (Dungey 1961; Deng & Matsumoto 2001; Oieroset et al. 2001; Burch et al. 2016; Torbert et al. 2018; Lu et al. 2022a). In the magnetotail, the current sheet is formed as the plasmas from the southern and northern lobes are convected toward the neutral plane, where the plasma parameters on two sides of the formed current sheet are almost the same, and symmetric reconnection occurs (McPherron 1991; Nagai et al. 2001; Angelopoulos et al. 2008; Sergeev et al. 2011; Lu et al. 2015, 2020b;

Wang et al. 2016). At the magnetopause, the current sheet is formed between the magnetosheath plasma with a southward component of magnetic field and the magnetospheric plasma with a northward component of magnetic field, where the parameters on the two sides of the current sheet are different and the occurring reconnection is asymmetric (Russell & Elphic 1978; Lee & Fu 1985; Scholer 1988; Mozer et al. 2008; Wang et al. 2017, 2020; Guo et al. 2021). The characteristics of both symmetric and asymmetric reconnection have been thoroughly studied with satellite observations and kinetic simulations (e.g., Ma & Bhattacharjee 2001; Pritchett 2001, 2008; Eastwood et al. 2010; Huang et al. 2010; Lu et al. 2010; Malakit et al. 2010; Hesse et al. 2014; Burch et al. 2016; Peng et al. 2017; Zhang et al. 2017; Torbert et al. 2018; Sang et al. 2019).

Another site at the Earth's magnetosphere where magnetic reconnection may occur is the downstream region of the bow shock. The bow shock is formed due to the interactions of the high-speed solar wind with the magnetosphere (Sagdeev 1966; Leory et al. 1982; Russell et al. 1982; Tsurutani & Stone 1985; Lembege & Dawson 1987; Yang et al. 2009). Retino et al. (2007) reported the first reconnection event in the magnetosheath with Cluster observations, where an ion diffusion region is identified, and they proposed that magnetic reconnection occurs in the current sheet formed due to plasma turbulence. More reconnection events have recently been observed with the high-resolution measurements provided by the Magnetospheric Multiscale spacecraft, and the width of the



Original content from this work may be used under the terms of the [Creative Commons Attribution 4.0 licence](https://creativecommons.org/licenses/by/4.0/). Any further distribution of this work must maintain attribution to the author(s) and the title of the work, journal citation and DOI.

associated current sheets ranges from the ion kinetic scale to the electron kinetic scale (Yordanova et al. 2016; Vörös et al. 2017; Phan et al. 2018; Gingell et al. 2019, 2020; Stawarz et al. 2019; Wang et al. 2019, 2021; Xu et al. 2023). Most of these reconnection events have been observed downstream of a quasi-parallel shock, which indicates that magnetic reconnection may occur ubiquitously in the quasi-parallel-shocked magnetosheath. In a quasi-parallel shock, the angle between the shock normal and the upstream magnetic field ( $\theta_{Bn}$ ) is smaller than  $45^\circ$ , and both the upstream and downstream are full of large-amplitude electromagnetic plasma waves (Winske et al. 1990; Scholer & Burgess 1992; Schwartz et al. 1992; Shan et al. 2014, 2020; Wu et al. 2015; Hao et al. 2016).

Kinetic simulations have also revealed the occurrence of magnetic reconnection in the transition region and downstream of the quasi-parallel shock (Bessho et al. 2019, 2020, 2023; Lu et al. 2020a; Gingell et al. 2023). With a global hybrid simulation model, Lu et al. (2020a) studied the generation of the bow shock due to the interaction between the high-speed solar wind and the Earth’s magnetosphere. They found that magnetic reconnection is initiated in current sheets downstream of a quasi-parallel shock, and they proposed that these current sheets are formed after the upstream large-amplitude low-frequency plasma waves penetrate the shock front and are then compressed. Magnetic reconnection induces a bidirectional high-speed ion flow (in the frame moving with an X-line) in the outflow region, and several flux ropes with an extension of about several Earth radii are produced in such a process. The upstream large-amplitude low-frequency plasma waves have been indicated to be magnetosonic waves excited due to the interaction between the solar wind and the reflected ions by the shock front and the upstream plasma (Scholer & Terasawa 1990; Winske et al. 1990; Su et al. 2012; Hao et al. 2016, 2021). The interaction can cause both resonant and nonresonant ion–ion beam instabilities in the upstream (Gary et al. 1984; Gary 1991; Akimoto et al. 1993; Scholer et al. 1997; Wang & Lin 2003). The plasma waves excited by the resonant ion–ion beam instability propagate toward the upstream in the upstream plasma frame and the wavelength is tens of ion inertial lengths, while the waves excited by the nonresonant ion–ion beam instability propagate toward the shock front in the upstream plasma frame and the wavelength is several ion inertial lengths. By performing a local two-dimensional (2D) particle-in-cell (PIC) simulation of a quasi-parallel shock, Bessho et al. (2020, 2023) found that magnetic reconnection can occur in the transition region after the excited plasma waves in the upstream penetrate into the downstream, where both ion and electron-scale magnetic islands are formed. They further found that although both the nonresonant and resonant ion–ion instabilities are excited, the nonresonant ion–ion instability is the dominant wave mode (Bessho et al. 2023). However, both kinetic simulations and satellite observations of quasi-parallel shocks have indicated that the dominant waves in the foreshock are excited by the resonant ion–ion instability (Hoppe & Russell 1983; Eastwood et al. 2005; Hobar et al. 2007). The large-amplitude low-frequency waves corresponding to the resonant ion–ion instability are brought toward the shock by the upstream plasma flow and interact with the shock, and then a new shock front is formed. This process is called shock reformation (Burgess 1989; Winske et al. 1990; Su et al. 2012; Hao et al. 2017), and to well resolve the shock reformation, one requires a longer time than that of

$20\Omega_{i0}^{-1}$  (where  $\Omega_{i0}$  is the ion gyrofrequency in the upstream) in Bessho et al. (2023).

In this paper, with a local 2D PIC simulation model, we study the long-time evolution of a quasi-parallel shock (near  $100\Omega_{i0}^{-1}$ ). We find that the waves excited in the upstream by the reflected ions correspond to the resonant ion–ion beam instability. The amplitude of the plasma waves increases continuously when they approach the shock, and then a new shock front is formed after they interact with the shock. The cycle period of such a kind of shock reformation is about  $12\Omega_{i0}^{-1}$ . When these large-amplitude low-frequency plasma waves penetrate the shock, the current sheets are generated in the shock transition region and magnetic reconnection consequently occurs.

## 2. Simulation Model

The software named EPOCH (Arber et al. 2015), which is an open-source electromagnetic 2D PIC simulation code, is used in this paper to study the characteristics of the quasi-parallel shock. The shock is formed by the injection method, where particles are injected from the left side of the simulation boundary (at  $x = 0$ ) with a speed  $V_{in} = 7V_{A0}$  (where  $V_{A0}$  is the Alfvén speed based on the upstream plasma density  $n_0$  and magnetic field  $B_0$ ) and a specular reflection for particles is used in the right boundary ( $x = L_x$ , where  $L_x$  is the size of the simulation domain in the  $x$ -direction). The formed shock propagates toward the left (the  $-x$ -direction). The 2D simulation is performed in the  $x - y$  plane, and the ambient magnetic field  $\mathbf{B}_0 = B_0(\cos\theta_{Bn}\mathbf{i}_x + \sin\theta_{Bn}\mathbf{i}_y)$ , where  $\theta_{Bn}$  is the shock normal angle. In our simulation, we choose  $\theta_{Bn} = 20^\circ$ , therefore the shock is quasi-parallel. Periodic boundary conditions for both electromagnetic fields and particles are applied in the  $y$ -direction.

The domain size of the simulation is  $L_x \times L_y = 1800d_{i0} \times 160d_{i0}$  (where  $d_{i0} = \frac{c}{\omega_{pi,0}}$  is the ion inertial length, and  $\omega_{pi,0} = \sqrt{\frac{n_0 e^2}{m_i \epsilon_0}}$  is the ion plasma frequency based on the upstream plasma density  $n_0$ ). The grid number is  $n_x \times n_y = 90,000 \times 8000$ , and the grid size is  $\Delta x = \Delta y = 0.02d_{i0}$ . Initially, there are 50 ions and electrons in each cell, and the ion-to-electron mass ratio is  $\frac{m_i}{m_e} = 100$ . The time step is  $\Omega_{i0}\Delta t = 0.001$ . The light speed is  $\frac{c}{V_{A0}} = 28$ . The plasma beta values in the upstream are  $\beta_{i0} = 0.1$ ,  $\beta_{e0} = 0.3$ .

## 3. Simulation Results

### 3.1. Upstream Plasma Waves and Shock Reformation

In order to identify the time evolution of the quasi-parallel shock, we plot in Figure 1 the time sequences of the profile of the magnetic field  $\bar{B}_t$  (where  $\bar{B}_t$  is the average value of the total magnetic field  $B_t = \sqrt{B_x^2 + B_y^2 + B_z^2}$  along the  $y$ -direction) versus  $x$  from  $\Omega_{i0}t = 55$  to 85. Note that the time separation between the profiles is  $\Omega_{i0}t = 1$ . In our simulation, in order to eliminate the effects from reflected ions on the right boundary on the upstream plasma waves, we focus on the evolution of these waves after  $\Omega_{i0}t = 55$ , when the shock front is far away from the right boundary. In the upstream, there exist large-amplitude low-frequency plasma waves, and the wavelength is about  $75d_{i0}$ . These waves are brought by the incident upstream plasma flow toward the shock front, and a new shock front is formed when the waves approach and coalesce with the shock front. This kind

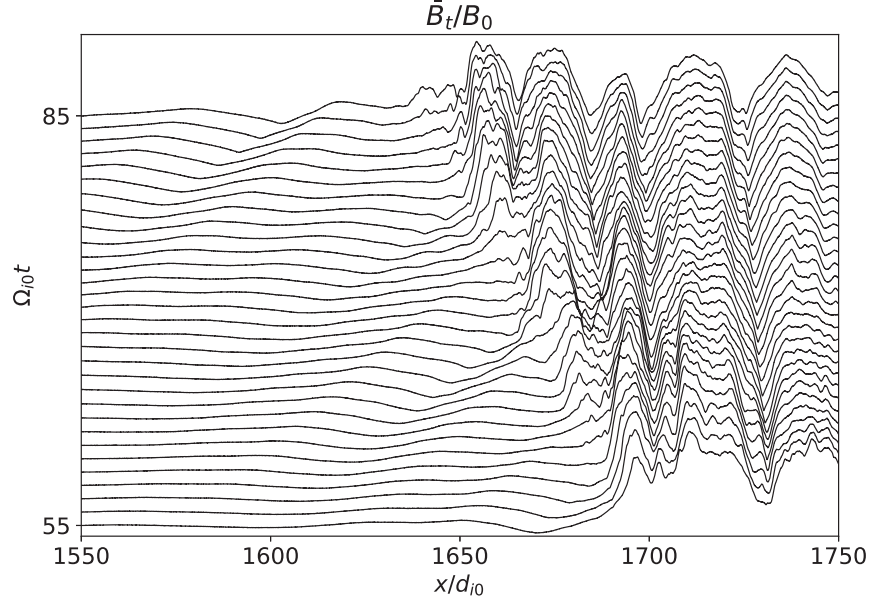


**Figure 1.** The time sequences of the profile of the magnetic field  $\bar{B}_t$  (where  $\bar{B}_t$  is the average value of the total magnetic field  $B_t = \sqrt{B_x^2 + B_y^2 + B_z^2}$  along the y-direction) vs.  $x$  from  $\Omega_{i0}t = 55$  to 85. Note that the time separation between the profiles is  $\Omega_{i0}t = 1$ .

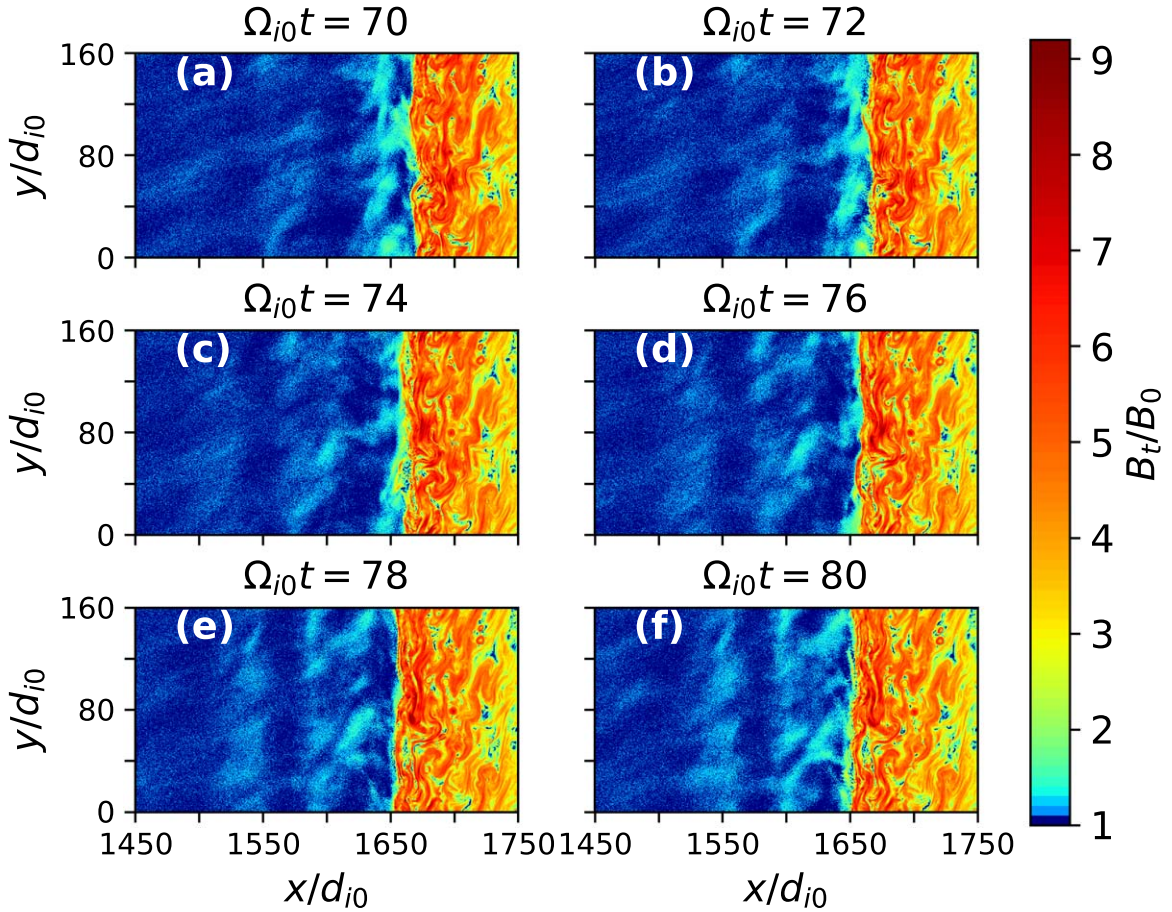


**Figure 2.** The total magnetic field  $B_t$  at  $\Omega_{i0}t =$  (a)70, (b)72, (c)74, (d)76, (e)78, and (f)80. These time sequences correspond to one reformation cycle.

of process is cyclic, which is called shock reformation, and the period is about  $12\Omega_{i0}^{-1}$ . The reformation process of the shock can be exhibited more clearly in Figure 2, which shows the total magnetic field  $B_t$  at  $\Omega_{i0}t =$  (a)70, (b)72, (c)74, (d)76, (e)78, and

(f)80. These time sequences correspond to one reformation cycle. At  $\Omega_{i0}t = 70$ , the shock front is located at around  $x = 1668d_{i0}$ , and there exist large-amplitude plasma waves in the upstream. If we follow the magnetic structure around

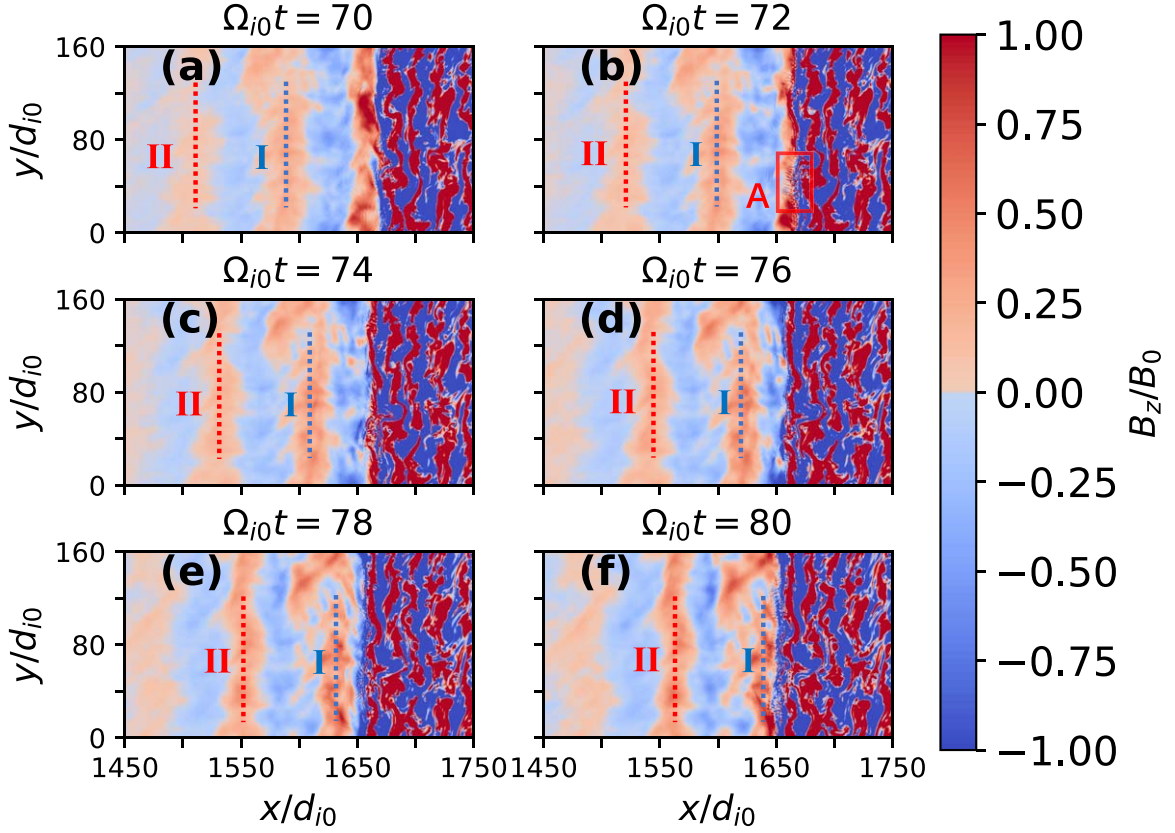


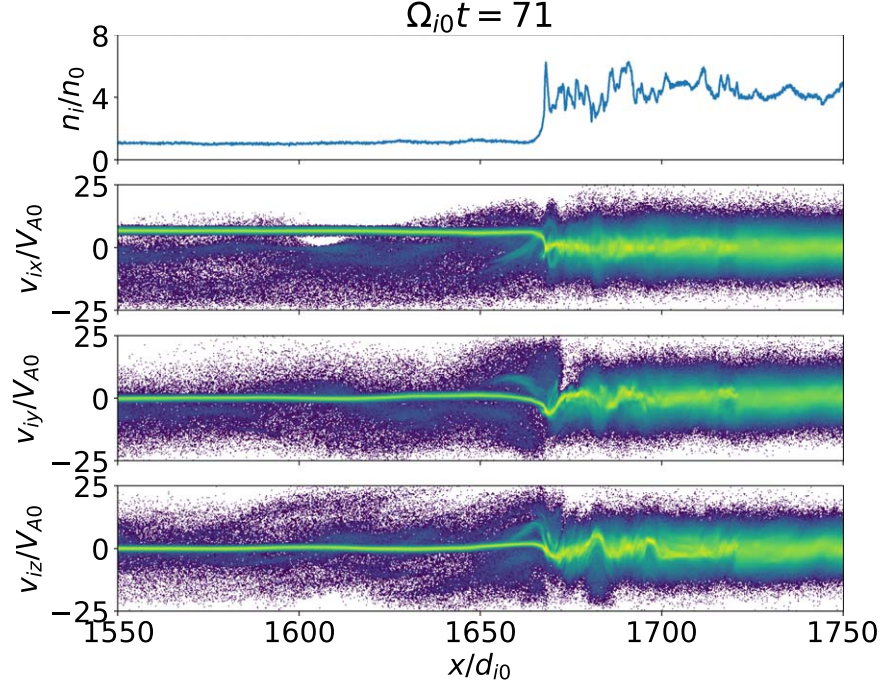
**Figure 3.** The magnetic field  $B_z$  at  $\Omega_{i0}t =$  (a) 70, (b) 72, (c) 74, (d) 76, (e) 78, and (f) 80. “I” and “II” represent two peaks of the upstream plasma waves.

$x = 1646d_{i0}$  at  $\Omega_{i0}t = 70$ , it is easy to find that the structure is approaching toward the shock front and it begins to interact with the shock front at about  $\Omega_{i0}t = 72$ . At about  $\Omega_{i0}t = 80$ , the magnetic structure merges with the shock front, and a new shock front is formed at around  $x = 1650d_{i0}$ . Therefore, the shock front propagates toward to the  $-x$ -direction with an average velocity of about  $1.8V_{A0}$ . In the shock frame, the velocity of the upstream plasma flow is about  $8.8V_{A0}$ , and the Alfvén Mach number is about 8.8. The reformation of a quasi-parallel shock has been thoroughly studied with kinetic simulations, and similar characteristics have been obtained (Burgess 1989; Tsubouchi & Lembege 2004; Su et al. 2012; Hao et al. 2017).

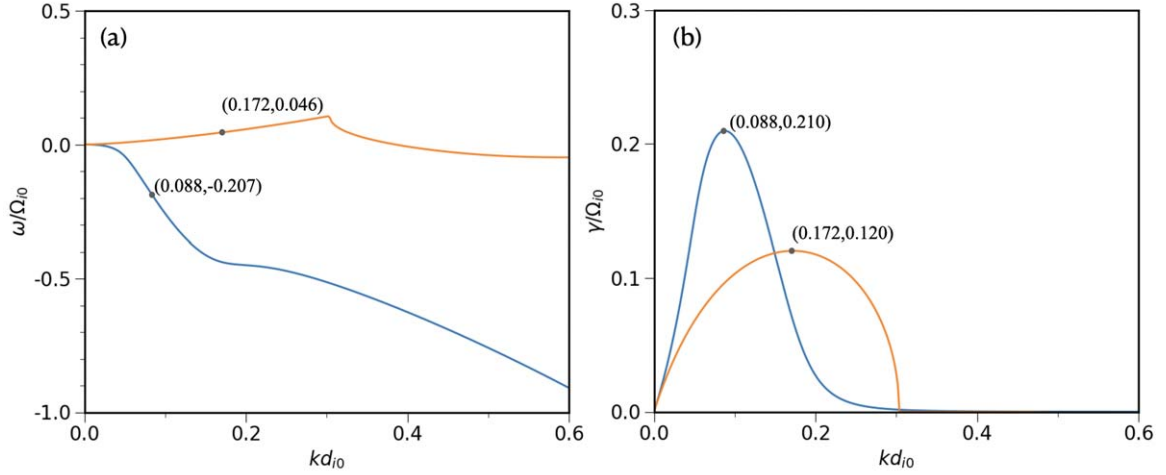
The characteristics of the plasma waves in the upstream can be exhibited more clearly in Figure 3, which plots the magnetic field  $B_z$  at  $\Omega_{i0}t =$  (a) 70, (b) 72, (c) 74, (d) 76, (e) 78, and (f) 80. In the figure, “I” and “II” represent two peaks of the upstream plasma waves. The wavelength of the upstream plasma waves can clearly be seen to be about  $75d_{i0}$ , and the wavenumber is about  $0.084d_{i0}^{-1}$ . The waves propagate almost along the  $+x$ -direction with a velocity of about  $5.2V_{A0}$ . Considering that the upstream plasma flow moves along the  $+x$ -direction with a velocity of  $7.0V_{A0}$ , the plasma waves propagate toward the  $-x$ -direction and the phase velocity is about  $1.8V_{A0}$  in the upstream plasma frame. The frequency of the plasma waves is estimated to be about  $0.15\Omega_{i0}$  in the upstream plasma frame, and the waves have a right-hand polarization. Besides these low-frequency plasma waves, there also exist plasma waves of another kind, with a much smaller wavelength in the ramp of the shock, which are denoted by “A” in Figure 3(b). We will analyze this kind of plasma wave later, in Figure 6.

Figure 4 shows the profiles of the ion number density  $n_i$  along the line  $y = 80d_{i0}$  and the scatter plot of the velocities ( $v_{ix}$ ,  $v_{iy}$ , and  $v_{iz}$ ) for the particles from  $y = 79.5d_{i0}$  to  $80.5d_{i0}$  at  $\Omega_{i0}t = 71$ . The shock front is located at around  $x = 1668d_{i0}$ . In the upstream, there exist two plasma populations: one corresponds to the upstream plasma, which flows toward the  $+x$ -direction with a velocity of  $7.0V_{A0}$ ; the other is the ions reflected around the shock front, which move toward the  $-x$ -direction with a velocity of about  $-6.1V_{A0}$ . The number of reflected ions becomes less and less farther upstream, accounting for about 3% of total particles around  $x = 1600d_{i0}$ . The upstream plasma waves are excited by the plasma beam comprised of the reflected ions, and the reflected ions are scattered by the upstream plasma waves to form diffuse superthermal ions (Scholer 1990; Su et al. 2012; Wu et al. 2015). In the upstream plasma frame, the beam velocity is about  $-13.1V_{A0}$ , and the frequency and wavevector are about  $\omega = 0.15\Omega_{i0}$  and  $k = 0.084d_{i0}^{-1}$ , respectively. They are resonant magnetosonic waves excited by the reflected ions due to the ion–ion beam instability because they satisfy the resonant condition  $\omega - kV_b \approx -\Omega_{i0}$ . In Figure 5, we plot the dispersion relation of the ion–ion beam instabilities in the upstream plasma frame with the parameters obtained from the simulation by performing the dispersion equation solver BO (Xie 2019). The dominant wave mode is excited by the resonant ion–ion beam instability, with the maximum growth rate about  $0.21\Omega_{i0}$  propagating along the  $-x$ -direction, and its frequency and wavenumber are about  $\omega = 0.207\Omega_{i0}$  and  $k = 0.088d_{i0}^{-1}$ , which are consistent with our simulation results.

In order to exhibit these plasma waves in the region denoted by “A” in Figure 3(b) more clearly, we plot in Figure 6 the



**Figure 4.** The profiles of the ion number density  $n_i$  along the line  $y = 80d_{i0}$  and the scatter plot of the velocities ( $v_{ix}$ ,  $v_{iy}$ , and  $v_{iz}$ ) for the particles from  $y = 79.5d_{i0}$  to  $80.5d_{i0}$  at  $\Omega_{i0}t = 71$ . The shock front is located at around  $x = 1675d_{i0}$ .



**Figure 5.** The dispersion relation of the ion–ion beam instabilities in the upstream plasma frame with the parameters obtained from the simulation. (a) The relation between the frequency ( $\omega$ ) and the wavenumber ( $k$ ). (b) The relation between the growth ( $\gamma$ ) and the wavenumber ( $k$ ). The blue and yellow lines correspond to the resonant and nonresonant wave modes, respectively. The positive and negative values of the frequency mean that the waves propagate along the  $+x$ - and  $-x$ -directions. The angle between the ambient magnetic field and the  $+x$ -direction is  $20^\circ$ . The ion beam contains 3% of the total ion density, and its bulk velocity is  $13.1V_{A0}$  along the  $-x$ -direction.

enlarged view of the magnetic field  $B_z$  at  $\Omega_{i0}t =$  (a)71.3, (b) 71.4, (c)72, and (d)73.6. The magnetic field lines in the  $x - y$  plane are also plotted with solid lines in the figure. The shock front is at around  $x = 1668d_{i0}$ , and obvious plasma waves can be found in the shock ramp. The wavelength is about  $2.0d_{i0}$ , which is about 2.5 local ion inertial lengths, because the plasma density is enhanced in the ramp region. In the local plasma frame, the waves propagate toward the shock front with an angle of about  $78^\circ$  with respect to the  $x$ -direction, which is about  $43^\circ$  related to the local magnetic field with a phase velocity of about  $1.0V_{A0}$ . In the region with the existence of these plasma waves, the upstream plasma flow begins to slow

down, and the density of the reflected ions accounts for about 13% of the total particles and is much larger than that in the upstream. In general, when the percentage of the beam density is sufficiently large ( $\sim 10\%$ ), the nonresonant ion–ion beam instability becomes more important than the resonant one (Akimoto et al. 1993). As shown in Figure 4, the plasma flow of the reflected ions is much more complicated than that in the upstream. Although its velocity along the  $-x$ -direction can be estimated to be about  $-4.3V_{A0}$ , it also has the  $y$ - and  $z$ -components. It is difficult to calculate the dispersion relation because of the complicated plasma flow of the reflected ions and the nonuniformity of the magnetic field. However, we

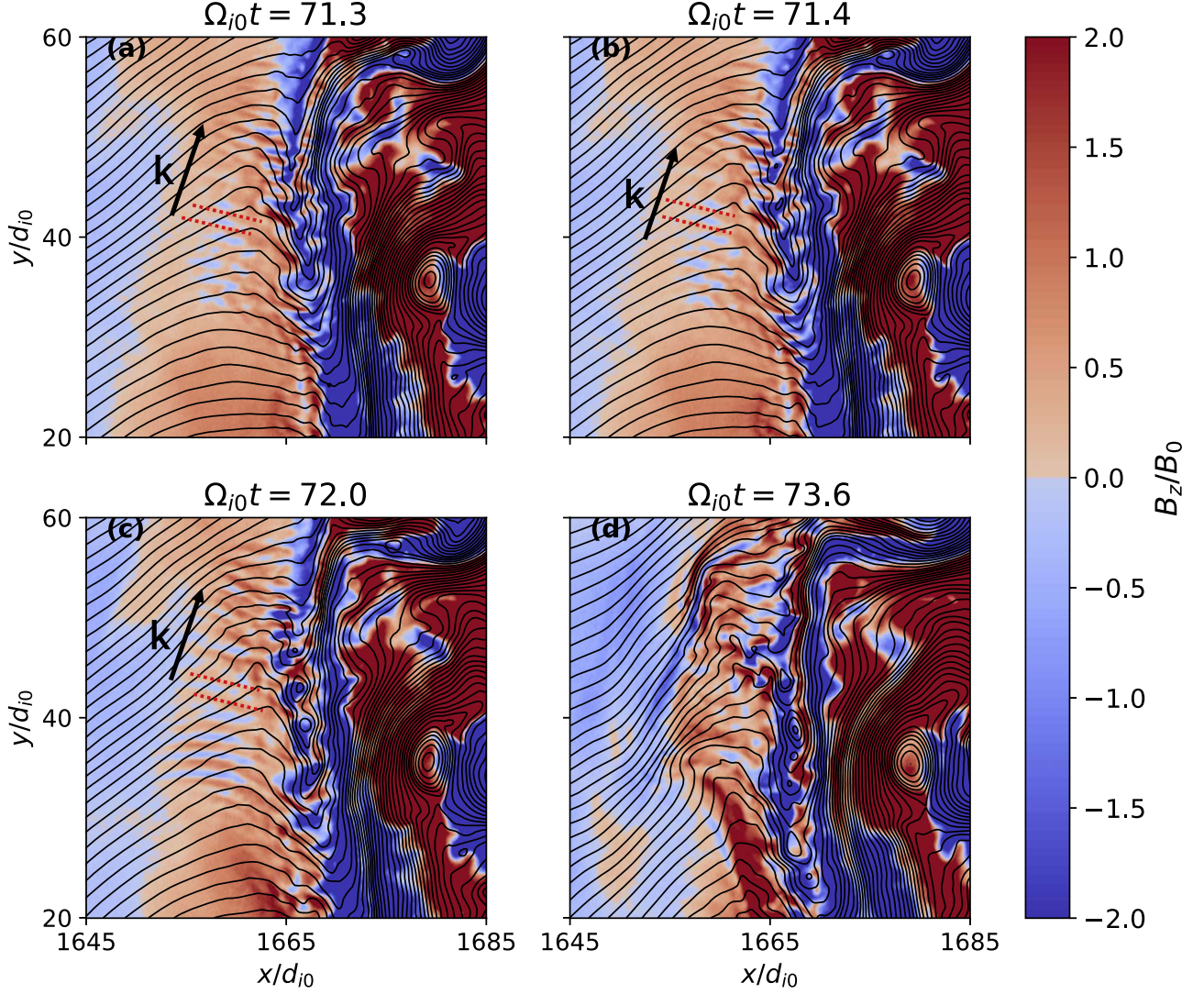


**Figure 6.** The enlarged view of the magnetic field  $B_z$  in the region denoted by “A” (Region A) in Figure 3(b) at  $\Omega_{i0}t =$  (a)71.3, (b)71.4, (c)72, (d)73.6. The magnetic field lines in the  $x - y$  plane are also plotted with the solid lines in the figure.

think that the plasma waves are excited by the nonresonant ion–ion beam instability, based on the wavelength and propagation direction of the excited plasma waves.

### 3.2. Formation of Current Sheets and Reconnection in the Transition Region

Figure 7 shows the current density in the  $z$ -direction  $J_z$  at  $\Omega_{i0}t =$  (a)70, (b)72, (c)74, (d)76, (e)78, and (f)80. The solid lines in the figure are the magnetic field lines in the  $x - y$  plane, and these time sequences correspond to one reformation cycle. Together with Figure 2, we can find that in the upstream the magnetic field lines are distorted and accompanied with the plasma waves. When these large-amplitude plasma waves penetrate into the downstream of the shock, the waves are compressed and the magnetic field lines become more distorted. At last, intense current sheets are formed in the transition region, and magnetic islands are generated in these current sheets, indicating that magnetic reconnection occurs. This process can be easily identified in Figure 8, which shows the enlarged view of the region denoted by “B” in Figure 7. At  $\Omega_{i0}t = 70$ , there is one plasma waveform in the upstream. It

interacts with the shock front at about  $\Omega_{i0}t = 72$ , and one current sheet is formed in the transition region of the shock. At about  $\Omega_{i0}t = 74$ , there form two current sheets in the transition region. Then magnetic reconnection occurs in one of the current sheets, and a magnetic island is generated at around  $y = 128d_{i0}$  at  $\Omega_{i0}t = 75$ . The magnetic island subsequently grows larger and larger, and simultaneously it moves upward slowly.

The characteristics of magnetic reconnection that occur in Region B can be seen clearly in Figure 9, which plots (a) the ion bulk velocity  $V_{iy}$ , (b) the electron bulk velocity  $V_{ey}$ , (c) the energy dissipation  $j_z E_z$ , (d) the magnetic field  $B_z$ , and (e) the ion and electron bulk velocities along the center of the current sheet (denoted by the dashed lines in Figures 9(a) and (b)) of Region B at  $\Omega_{i0}t = 78$ . A magnetic island is located at around  $y = 129d_{i0}$ , and there exists an X-line just below the magnetic island. The half-width of the current sheet is about  $1.0d_{i0}$  (about 2.3 local ion inertial lengths), while that of the magnetic island is about  $2.0d_{i0}$  (about 4.7 local ion inertial lengths). Energy dissipation  $j_z E_z$  caused by magnetic reconnection can be found around the X-line, and it is not as strong as that in the Harris current sheet, which may be caused by the strong background

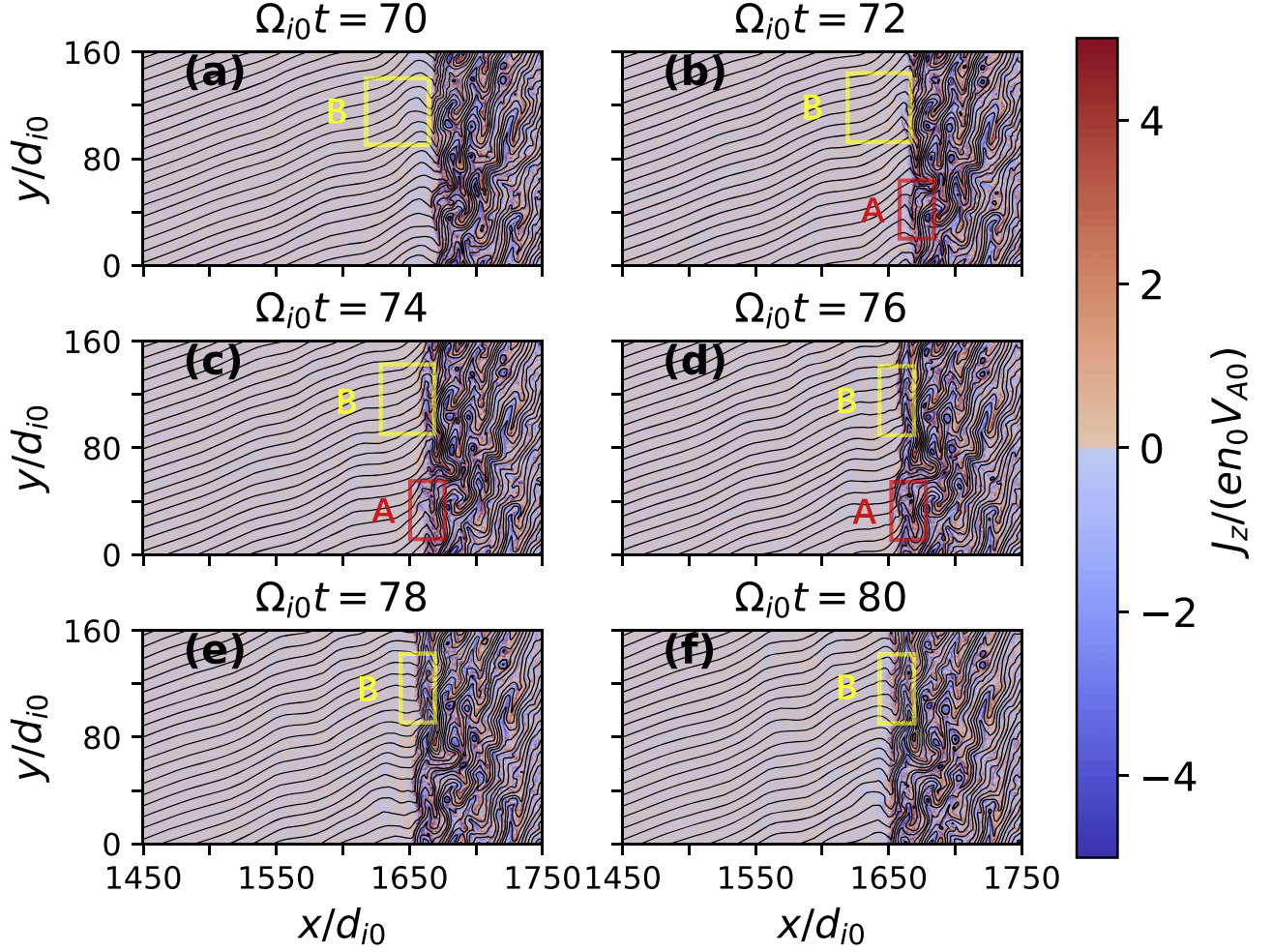


**Figure 7.** The current density in the  $z$ -direction  $J_z$  at  $\Omega_{i0}t =$  (a)70, (b)72, (c)74, (d)76, (e)78, and (f)80. The solid lines are the magnetic field lines in the  $x - y$  plane, and these time sequences correspond to one reformation cycle.

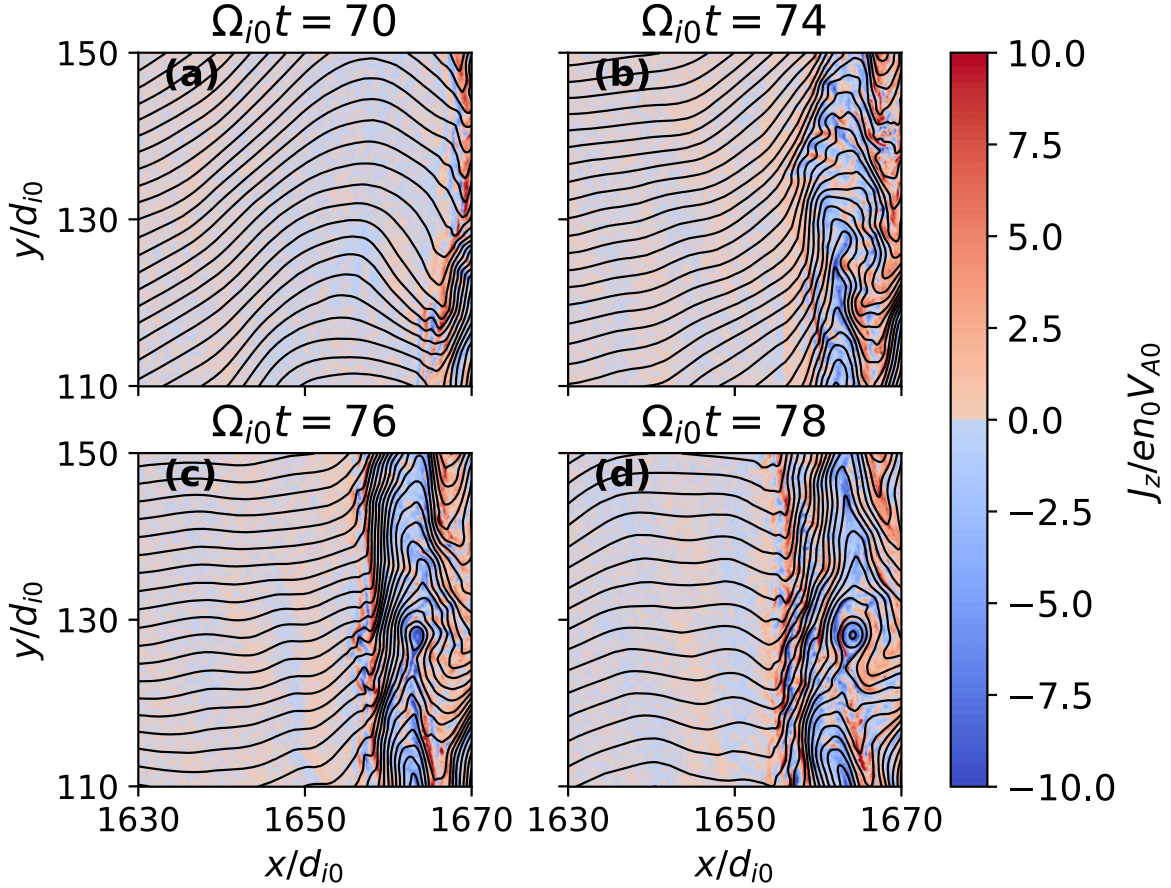
plasma flow in the downstream. Magnetic reconnection also leads to a high-speed flow in the outflow region. The difference of the ion flow velocity between the two outflow regions is about  $1.8V_{A0}$ , while that of the electron flow velocity is about  $4.0V_{A0}$ . Therefore, ion-coupling magnetic reconnection occurs in Region B.

Figure 10 shows the current density in the  $z$ -direction  $J_z$  within region A (denoted in Figure 3 and 7) at  $\Omega_{i0}t =$  (a)71.3, (b)71.4, (c)72.0, and (d)73.6. Here, the solid lines are the magnetic field lines in the  $x - y$  plane. Together with Figure 6, we can find when the high-frequency waves in the ramp region interact with the shock front, and the current sheet in the transition region is twisted and broken into several segments. Several magnetic islands whose half-widths range from 0.2 to  $1.0d_{i0}$  (or 0.28 to 1.4 local inertial lengths) are formed, and the half-width of the current sheet can also be as small as about  $0.2d_{i0}$  (or about  $2.0d_{e0}$ ). Because in our simulation we use the ion-to-electron mass ratio  $\frac{m_i}{m_e} = 100$ , it is difficult to distinguish whether the size of these magnetic islands can be small to the electron inertial length. The characteristics of magnetic reconnection are shown in Figure 11, which plots (a) the ion bulk velocity  $V_{iy}$ , (b) the electron bulk velocity  $V_{ey}$ , (c) the energy dissipation  $j_z E_z$ , (d) the magnetic field  $B_z$ , and (e) the ion and electron bulk velocity along the center of the current sheet (denoted by the dashed lines in Figures 11(a) and (b)) of

Region A at  $\Omega_{i0}t = 72.3$ . The presence of magnetic islands separates the current sheet into several segments, where there exists obvious energy dissipation  $j_z E_z$ . The plasma has an average flow with a speed of about  $1.0V_{A0}$  along the  $-y$ -direction. From the velocity difference between the upper and lower parts of the current sheet, we can estimate the speed of the ion outflow caused by magnetic reconnection as about  $1.0V_{A0}$ . Around the X-lines, like those denoted by “X1,” “X2,” “X3,” and “X4” in Figure 11(e), we can find large fluctuations of the electron outflow, which may be larger the Alfvén speed. Around some X-lines, like those denoted by “X3” and “X4,” the ion flow almost does not change. This is a characteristic of electron-only reconnection (Phan et al. 2018; Wang et al. 2018; Pyakurel et al. 2019; Lu et al. 2020b, 2022b; Guan et al. 2023), and it implies that electron-only reconnection may occur in this kind of current sheet.

### 3.3. Conclusions and Discussion

In this paper, by performing a 2D PIC simulation of a quasi-parallel shock, we investigate the evolution from upstream low-frequency plasma waves to current sheets in the downstream, where magnetic reconnection at last occurs. In the upstream, the dominant plasma waves, which belong to magnetosonic waves, are excited by the reflected ions due to the resonant ion-ion beam instability. The wavelength of the excited plasma waves is



**Figure 8.** The enlarged of view of the region denoted by “B” in Figure 7.

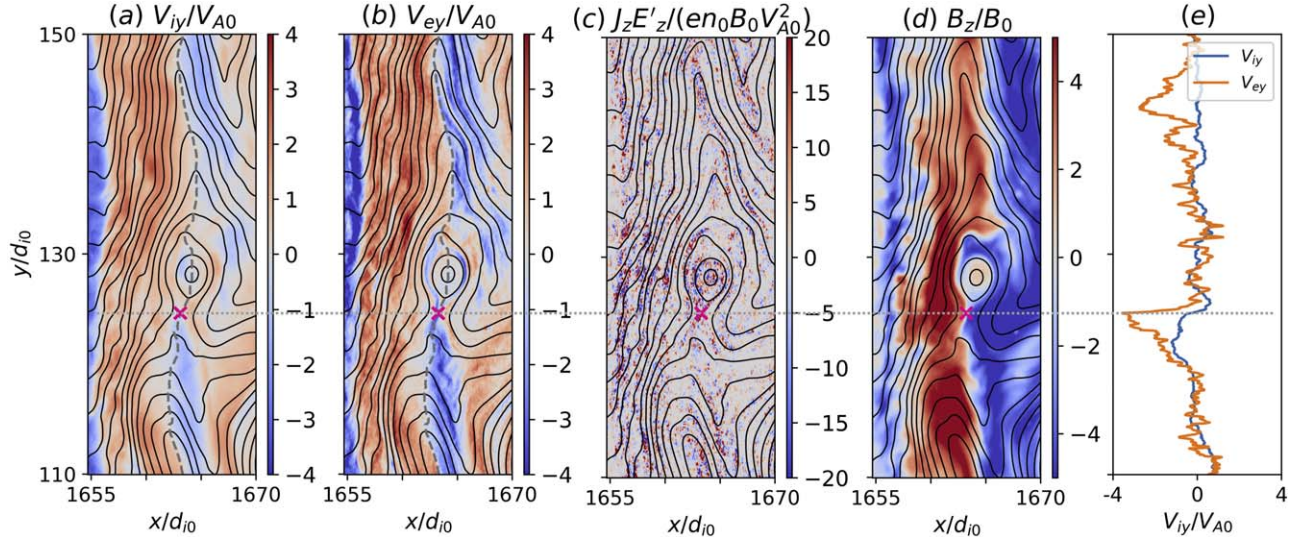


**Figure 9.** (a) The ion bulk velocity  $V_{iy}$ . (b) The electron bulk velocity  $V_{ey}$ . (c) The energy dissipation  $j_z E'_z$ . (d) The magnetic field  $B_z$ . (e) The ion and electron bulk velocities along the center of the current sheet (denoted by the dashed lines in Figures 9(a) and (b)) of Region B at  $\Omega_{i0} t = 78$ .

about  $75d_{i0}$ , while the frequency is about  $0.15\Omega_{i0}$  in the upstream plasma frame. In the upstream plasma frame, the plasma waves try to propagate toward the upstream with a phase velocity of about 1.5 Alfvén speed, but they are brought toward the shock front by the upstream plasma flow, because the flow velocity of the upstream plasma is much larger than the phase velocity of the plasma waves. The interaction between the

upstream plasma waves and the shock causes the cyclic reformation of the shock front with a period of about  $12\Omega_{i0}^{-1}$ . When the upstream plasma waves cross the shock front into the downstream, they are compressed, and then evolve into current sheets in the transition region. Simultaneously, there still exist plasma waves of another kind, with a wavelength of about  $2.0d_{i0}$  in the ramp region, which propagate toward the shock front in



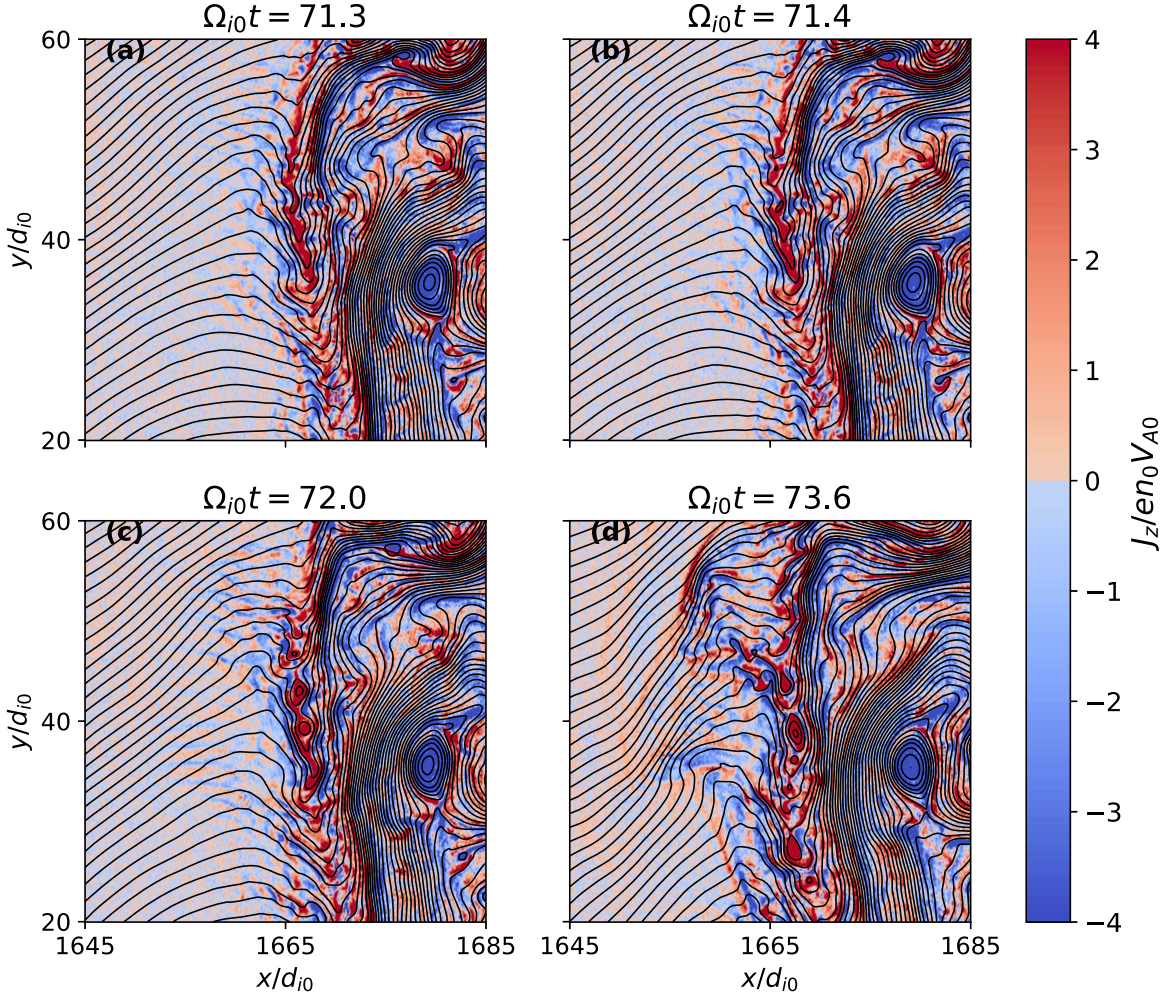


**Figure 10.** The current density in the  $z$ -direction  $J_z$  within region A (denoted in Figure 3 and 7) at  $\Omega_{i0}t =$  (a)71.3, (b)71.4, (c)72.0, and (d)73.6. The solid lines are the magnetic field lines in the  $x - y$  plane.

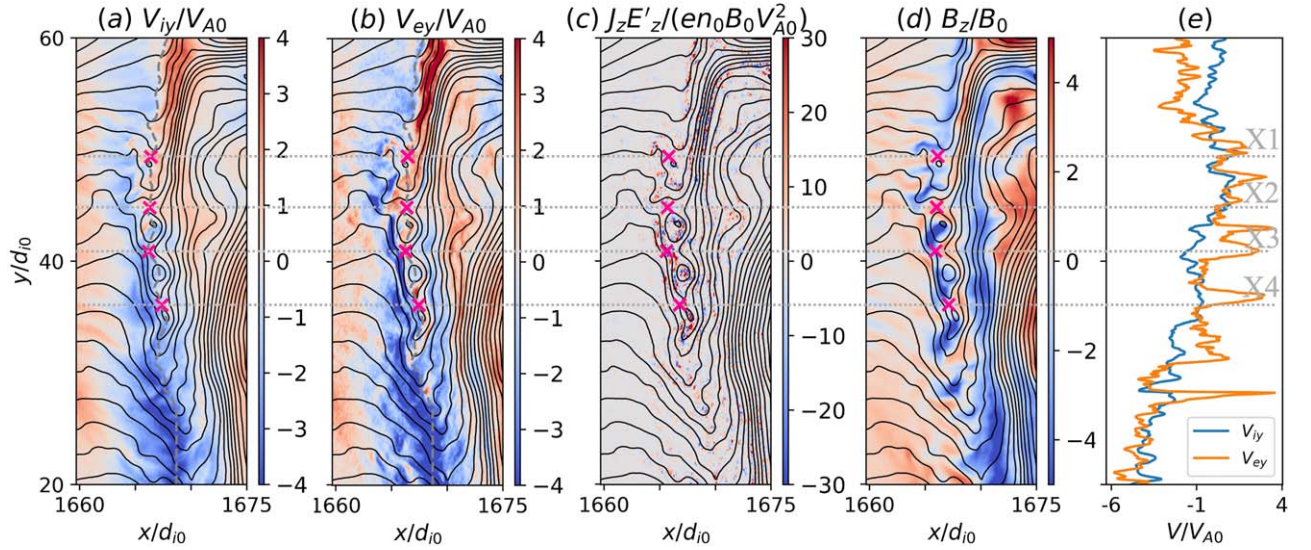


**Figure 11.** (a) The ion bulk velocity  $V_{iy}$ , (b) The electron bulk velocity  $V_{ey}$ , (c) The energy dissipation  $j_z E'_z / (en_0 B_0 V_{A0}^2)$ , (d) The magnetic field  $B_z$ , (e) The ion and electron bulk velocity along the center of the current sheet (denoted by the dashed lines in Figures 11(a) and (b)) of Region A at  $\Omega_{i0}t = 72.3$ .

the local plasma frame. When the waves enter the transition region, they break the current sheets into many segments, and at last may evolve into the electron scale. We cannot observe an

obvious change of ion flow around some X-lines produced by magnetic reconnection, and this implies that electron-only reconnection may occur in these current sheets.

Bessho et al. (2020, 2023) have also studied the upstream plasma waves and downstream magnetic reconnection in a quasi-parallel shock. Different from our simulation, they have only run the simulation for about  $20\Omega_{i0}^{-1}$ , and the dominant plasma waves in the upstream are excited by the nonresonant ion–ion beam instability, even though the low-frequency waves excited by the resonant ion–ion beam instability begin to appear at the end of their simulation. It is well known that both resonant and nonresonant ion–ion beam instabilities can be excited in a plasma beam system. In the plasma conditions of the Earth’s bow shock, the wavelength of the plasma waves excited by the resonant ion–ion beam instability is about tens of ion inertial lengths, which is much larger than that excited by the nonresonant ion–ion beam instability (about several ion inertial lengths). However, previous satellite observations and kinetic simulations of a quasi-parallel shock in the Earth’s bow shock have proved that the dominant upstream plasma waves belong to the resonant ion–ion beam instability (Eastwood et al. 2005; Hobar et al. 2007; Su et al. 2012). The difference may be because Bessho et al. (2023, 2023) have only run their simulation for about  $20\Omega_{i0}^{-1}$ . The shock front is very near to the boundary, which reflects the incident particles and produces the shock front, and this may artificially enhance the ion beam density. Simultaneously, even these ions reflected by the shock front can only move toward the upstream in a distance comparable to the wavelength of the dominant wave mode excited by the resonant ion–ion beam instability. Therefore, in Bessho et al. (2020, 2023), they can only observe the plasma waves (the wavelength is only several ion inertial lengths) excited by the nonresonant ion–ion beam instability, just like those excited in the ramp of the shock in our simulation.

The plasma parameters used in our simulation are very typical at the Earth’s bow shock, where the Alfvén Mach number is about 8.8. We found that the dominant plasma waves in the upstream are excited due to the resonant ion–ion beam instability. The wavelength of the plasma waves is  $\lambda \approx 75d_{i0}$  (the wavenumber is  $k \approx 0.084d_{i0}^{-1}$ ), and the frequency is  $\omega \approx 0.15\Omega_{i0}$  in the upstream plasma frame. Therefore, the wave frequency in the satellite frame is  $\omega' = |\omega - kV_{SW}| \approx 0.59\Omega_{i0}$ . The typical magnetic field of the solar wind at 1 au is about  $2nT$ , therefore we can calculate the wave period  $T = \frac{2\pi}{\omega'}$  in the satellite frame to be about 30 s. It is generally believed that the plasma waves with a period of around 30 s are the dominant foreshock waves observed by satellites in the upstream of the Earth’s bow shock (Eastwood et al. 2005; Hobar et al. 2007), which is consistent with that of the dominant plasma waves obtained in our simulation. Therefore, we believe that the current sheets downstream of a quasi-parallel shock are formed after the low-frequency waves excited due to the resonant ion–ion beam instability penetrate the shock front, and their width is about several ion inertial lengths. The plasma waves, which may be excited due to the nonresonant ion–ion beam instability around the ramp of the shock, break the current sheets into many segments. These segments may extend to the electron scale and may lead to the occurrence of electron-only reconnection.

### Acknowledgments

This work was supported by the National Natural Science Foundation of China (NSFC) grants 42150105, 42174181, 42188101 and 42274210, the National Key Research and Development Program of China (No. 2022YFA1604600), and the Strategic Priority Research Program of the Chinese Academy

of Sciences, grant No. XDB 41000000. We thank Professor Shan Wang at Peking University for help in calculating the dispersion relation of the ion–ion beam instabilities.

### ORCID iDs

Quanming Lu  <https://orcid.org/0000-0003-3041-2682>  
 Ao Guo  <https://orcid.org/0000-0002-7625-7625>  
 Zhongwei Yang  <https://orcid.org/0000-0002-1509-1529>  
 Rongsheng Wang  <https://orcid.org/0000-0002-9511-7660>  
 San Lu  <https://orcid.org/0000-0003-2248-5072>  
 Rui Chen  <https://orcid.org/0000-0002-4828-5709>

### References

- Akimoto, K., Winske, D., Gary, S. P., & Thomsen, M. F. 1993, *JGR*, **98**, 1419
- Angelopoulos, V., McFadden, J. P., Larson, D., et al. 2008, *Sci*, **321**, 931
- Arber, T. D., Bennett, K., Brady, C. S., et al. 2015, *PPCF*, **57**, 113001
- Bessho, N., Chen, L.-J., Hesse, M., et al. 2023, *ApJ*, **954**, 25
- Bessho, N., Chen, L.-J., Wang, S., et al. 2019, *GeoRL*, **46**, 9352
- Bessho, N., Chen, L.-J., Wang, S., et al. 2020, *PhPI*, **27**, 092901
- Birn, J., Drake, J. F., Shay, M. A., et al. 2001, *JGR*, **106**, 3715
- Birn, J., & Priest, E. R. 2007, *Reconnection of Magnetic Fields: Magnetohydrodynamics and Collisionless Theory and Observations* (Cambridge: Cambridge Univ. Press)
- Biskamp, D. 2000, *Magnetic Reconnection in Plasmas* (Cambridge: Cambridge Univ. Press)
- Burch, J. L., Moore, T. E., Torbert, R. B., & Giles, B. L. 2016, *SSRv*, **199**, 5
- Burgess, D. 1989, *GRL*, **16**, 345
- Deng, X. H., & Matsumoto, H. 2001, *Natur*, **410**, 557
- Dungey, J. W. 1961, *PhRvL*, **6**, 47
- Eastwood, J. P., Balogh, A., & Lucek 2005, *JGRA*, **110**, A11219
- Eastwood, J. P., Shay, M. A., Phan, T. D., & Øieroset, M. 2010, *PhRvL*, **104**, 205001
- Fu, X. R., Lu, Q. M., & Wang, S. 2006, *PhPI*, **13**, 012309
- Gary, S. P. 1991, *SSRv*, **56**, 373
- Gary, S. P., Smith, C. W., Lee, M. A., et al. 1984, *PhFI*, **27**, 1852
- Gingell, I., Schwartz, S. J., Eastwood, J. P., et al. 2019, *GeoRL*, **46**, 1177
- Gingell, I., Schwartz, S. J., Eastwood, J. P., et al. 2020, *JGRA*, **125**, e27119
- Gingell, I., Schwartz, S. J., Kucharek, H., et al. 2023, *PhPI*, **30**, 012902
- Guan, Y. D., Lu, Q. M., Lu, S., et al. 2023, *ApJ*, **958**, 172
- Guo, J., Lu, S., Lu, Q. M., et al. 2021, *JGRA*, **126**, e2021JA029388
- Hao, Y. F., Gao, X. L., Lu, Q. M., et al. 2017, *JGRA*, **122**, 6385
- Hao, Y. F., Lembege, B., & Lu, Q. M. 2016, *JGRA*, **121**, 2080
- Hao, Y. F., Lu, Q. M., Wu, D. J., et al. 2021, *ApJ*, **915**, 64
- Hesse, M., Aunai, N., Sibeck, D., & Birn, J. 2014, *GeoRL*, **41**, 8673
- Hobar, Y., Walker, S. N., Balikhin, M., et al. 2007, *JGRA*, **112**, A07202
- Hoppe, M. M., & Russell, C. T. 1983, *JGR*, **88**, 2021
- Huang, C., Lu, Q. M., & Wang, S. 2010, *PhPI*, **17**, 072306
- Lee, L. C., & Fu, Z. F. 1985, *GeoRL*, **12**, 105
- Lembege, B., & Dawson, J. M. 1987, *PhFI*, **30**, 1767
- Leory, M. M., Winske, D., Goodrich, C. C., et al. 1982, *JGR*, **87**, 5081
- Lu, Q. M., Fu, H. S., Wang, R. S., & Lu, S. 2022a, *ChPhB*, **31**, 089401
- Lu, Q. M., Huang, C., Xie, J. L., et al. 2010, *JGRA*, **115**, A11208
- Lu, Q. M., Wang, H. Y., Wang, X. Y., et al. 2020a, *GeoRL*, **47**, e2019GL085661
- Lu, S., Lu, Q. M., Lin, Y., et al. 2015, *JGRA*, **120**, 6286
- Lu, S., Lu, Q. M., Wang, R. S., et al. 2022b, *GeoRL*, **49**, e2022GL098547
- Lu, S., Wang, R. S., Lu, Q. M., et al. 2020b, *NatCo*, **11**, 5049
- Ma, Z. W., & Bhattacharjee, A. 2001, *JGR*, **106**, 3773
- Malakit, K., Shay, M. A., Cassak, P. A., & Bard, C. 2010, *JGRA*, **115**, A10223
- McPherron, R. L. 1991, in *Physical Processes Producing Magnetospheric Substorms and Magnetic Storms*, in Geomagnetism, ed. J. Jacobs (London: Academic), 593
- Mozer, F. S., Angelopoulos, V., Bonnell, J., et al. 2008, *GeoRL*, **35**, L17S04
- Nagai, T., Shinohara, I., Fujimoto, M., et al. 2001, *JGR*, **106**, 25929
- Øieroset, M., Phan, T. D., Fujimoto, M., et al. 2001, *Natur*, **412**, 414
- Parker, E. N. 1957, *JGR*, **62**, 509
- Peng, F. Z., Fu, H. S., Cao, J. B., et al. 2017, *JGRA*, **122**, 6349
- Phan, T. D., Eastwood, J. P., Shay, M. A., et al. 2018, *Natur*, **557**, 202
- Pritchett, P. L. 2001, *JGR*, **106**, 3783
- Pritchett, P. L. 2008, *JGRA*, **113**, A06210
- Pyakurel, P. S., Shay, M. A., Phan, T. D., et al. 2019, *PhPI*, **26**, 082307

- Retino, A., Sundkvist, D., Vaivads, A., et al. 2007, *NatPh*, **3**, 235
- Russell, C. T., & Elphic, R. C. 1978, *SSRv*, **22**, 681
- Russell, C. T., Hoppe, M. M., & Livesey, W. A. 1982, *Natur*, **296**, 45
- Sagdeev, R. Z. 1966, *RvPP*, **4**, 23
- Sang, L. L., Lu, Q. M., Wang, R. S., et al. 2019, *ApJ*, **877**, 155
- Scholer, M. 1988, *GeoRL*, **15**, 748
- Scholer, M. 1990, *GeoRL*, **17**, 1821
- Scholer, M., & Burgess, D. 1992, *JGR*, **97**, 8319
- Scholer, M., Kucharek, H., & Jayanti, V. 1997, *JGR*, **102**, 9821
- Scholer, M., & Terasawa, T. 1990, *GeoRL*, **17**, 119
- Schwartz, S. J., Burgess, D., Wilkinson, W. P., et al. 1992, *JGR*, **97**, 4209
- Sergeev, V., Angelopoulos, V., Kubyskhina, M., et al. 2011, *JGRA*, **116**, A00126
- Shan, L., Du, A., Tsurutani, B. T., et al. 2020, *ApJL*, **888**, L17
- Shan, L., Lu, Q. M., Wu, M., et al. 2014, *JGRA*, **119**, 237
- Stawarz, J. E., Eastwood, J. P., Phan, T. D., et al. 2019, *ApJL*, **877**, L37
- Su, Y. Q., Lu, Q. M., Huang, C., et al. 2012, *JGRA*, **117**, A08107
- Sweet, P. A. 1958, *The Neutral Point Theory of Solar Flares*//Lehnert B. *Electromagnetic Phenomena in Cosmical Physics* (Cambridge: Cambridge Univ. Press), 123
- Torbert, R. B., Burch, J. L., Phan, T. D., et al. 2018, *Sci*, **362**, 1391
- Tsubouchi, K., & Lembege, B. 2004, *JGRA*, **109**, A08107
- Tsurutani, B. T., & Stone, R. G. 1985, *Collisionless Shocks in the Heliosphere: A Tutorial Review*, Vol 34 (Washington, DC: American Geophysical Union)
- Vasyliunas, V. M. 1975, *RvGSP*, **1975**, 303
- Vörös, Z., Yordanova, E., Varsani, A., et al. 2017, *JGRA*, **122**, 11442
- Wang, R. S., Lu, Q. M., Lu, S., et al. 2020, *GeoRL*, **47**, e88761
- Wang, R. S., Lu, Q. M., Nakamura, R., et al. 2016, *NatPh*, **12**, 263
- Wang, R. S., Lu, Q. M., Nakamura, R., et al. 2018, *GeoRL*, **45**, 4542
- Wang, R. S., Nakamura, R., Lu, Q. M., et al. 2017, *PhRvL*, **118**, 175101
- Wang, S., Chen, L.-J., Bessho, N., et al. 2019, *GeoRL*, **46**, 562
- Wang, S., & Lu, Q. M. 2019, *Collisionless Magnetic Reconnection* (Beijing: Science Press)
- Wang, S. M., Wang, R. S., Lu, Q. M., et al. 2021, *GeoRL*, **48**, e94879
- Wang, X. Y., & Lin, Y. 2003, *PhPI*, **10**, 3528
- Winske, D., Omid, N., Quest, K. B., & Thomas, V. A. 1990, *JGR*, **95**, 18821
- Wu, M. Y., Hao, Y. F., Lu, Q. M., et al. 2015, *ApJ*, **808**, 2
- Xie, H. S. 2019, *CoPhC*, **244**, 343
- Xu, Q., Zhou, M., Ma, W., et al. 2023, *GeoRL*, **50**, e2022GL102523
- Yamada, M., Kulsrud, R., & Ji, H. T. 2010, *RvMP*, **82**, 603
- Yang, Z. W., Lu, Q. M., Lembege, B., & Wang, S. 2009, *JGRA*, **114**, A03111
- Yordanova, E., Vörös, Z., Varsani, A., et al. 2016, *GeoRL*, **43**, 5969
- Zhang, T. L., Lu, Q. M., Baumjohann, W., et al. 2012, *Sci*, **336**, 567
- Zhang, Y. C., Lavraud, B., Dai, L., et al. 2017, *JGRA*, **122**, 5277